Excited-State Energy Flow in Covalently Linked Multiporphyrin Arrays: The Essential Contribution of Energy Transfer between Nonadjacent Chromophores

Eve Hindin,[†,§] Robert A. Forties,[‡] Robert S. Loewe,[¶] Arounaguiry Ambroise,[¶] Christine Kirmaier,[†] David F. Bocian,[#] Jonathan S. Lindsey,[¶] Dewey Holten,*[,†] and Robert S. Knox[‡]

Department of Chemistry, Washington University, St. Louis, Missouri 63130-4889, Department of Physics and Astronomy, University of Rochester, Rochester, New York 14627-0171, Department of Chemistry, North Carolina State University, Raleigh, North Carolina 27695-8204, and Department of Chemistry, University of California, Riverside, California 92521-0403

Received: May 21, 2004

A series of multiporphyrin arrays has been studied to probe the contribution of energy transfer between second-neighbor ("nonadjacent") porphyrins and to determine the rate of energy transfer between identical porphyrins at adjacent sites. The arrays, organized in linear or branched architectures, contain up to 21 constituents, domains of 2−5 zinc porphyrins, and a single energy trap. The study has involved iterative cycles of molecular design, synthesis, determination of rates via transient absorption spectroscopy, and kinetic analysis. A rate constant of $(30 \pm 10\ \text{ps})^{-1}$ is deduced for bidirectional energy transfer between adjacent zinc porphyrins joined by a diphenylethyne linker. The value is $(50 \pm 10\ \text{ps})^{-1}$ when the porphyrin-linker internal rotation is hindered by *o,o′*-methyl groups on one aryl ring of the linker. Rates of nonadjacent energy transfers are typically only 5−10-fold less than the rates of adjacent transfers. Thus, the nonadjacent pathway has a significant impact on the overall rate of energy flow to the trap, even in architectures as small as triads. These findings provide information that will be essential for the rational design of multichromophore arrays whose function is to transfer excitation energy efficiently over large distances to a trap site.

Introduction

In photosynthetic antenna complexes, absorbed solar energy migrates among a large number (as many as 100−200) of identical chlorophyll molecules en route to the reaction center.[1] Such a multistep process is also operative in synthetic light-harvesting complexes whose multichromophore design draws inspiration from the natural system.[2−11] We have been exploring such surrogate light-harvesting systems comprised of multiple zinc porphyrins and a single embedded free base porphyrin trap, with adjacent constituents joined by diarylethyne linkers (Charts 1−3).[3] For each array, we have measured the effective time constant (τ_R) for the rise of excitation at the free base porphyrin following the excitation of one zinc porphyrin. The **Zn^{U}Fb** dyad,[12] **Zn^{U}Fb^{U}Zn** triad,[13] and **Zn$_4$Fb** pentad[14] are benchmark cases wherein excitation can reach the trap in a single step (Chart 1); the τ_R values for these arrays are all ∼20 ps. In the **Zn$_8$Fb** nonamer[15] (Chart 2) and the **Zn$_{20}$Fb** 21-mer[15] (Chart 3), the minimum number of steps from the most distant zinc porphyrin to the free base trap is two and three, respectively, with concomitant increases in the τ_R values to ∼100 and ∼300 ps, respectively. Chart 4 shows a related molecular wire in which excitation input at the perylene dye migrates through three zinc porphyrins before reaching the trap with a τ_R value of ∼170 ps.[16] In these arrays and a variety of others employing the diarylethyne linker, the porphyrins are weakly coupled electronically, so that key electronic properties of the monomeric building blocks (e.g., inherent photophysical properties) are retained in the arrays.[3] Despite the weak coupling, the energy transfer proceeds rapidly (picosecond regime) and efficiently (typically >90%), predominantly via a through-bond mechanism.

Our previous studies of multiporphyrin arrays have shown that the dominant pathway for energy flow is, as expected, the transfer between adjacent chromophores. However, direct transfer between second-neighbor ("nonadjacent") chromophores can also influence the overall energy-transfer dynamics and efficiency. The importance of nonadjacent energy transfer in covalently linked porphyrin arrays is illustrated by the energy flow in the triad shown in Chart 5. This triad, designated **Mg^{U}Zn^{U}Fb**, contains three different chromophores (magnesium, zinc, and free base porphyrins) with different excited-state energies. The diphenylethyne linker is unhindered (superscript **U**) toward internal rotation about the bonds with the porphyrins; this motif was chosen because we have demonstrated that torsional constraints such as *o*-methyl substituents slow energy transfer in multiporphyrin arrays.[3] Excitation of the central Zn porphyrin in the triad results in the branched, downhill through-bond energy transfer to the outside Mg and Fb porphyrins with rate constants that are comparable to those in the dyads **Zn^{U}Mg** [$\sim(9\ \text{ps})^{-1}$] and **Zn^{U}Fb** [$\sim(24\ \text{ps})^{-1}$] shown in Chart 6.[17] However, the energy on the Mg porphyrin resulting from this process (or direct excitation in a separate experiment) is ultimately transferred to the nonadjacent free base porphyrin with a rate constant of $\sim(170\ \text{ps})^{-1}$ at room temperature. This value changes very little at 80 K. Collectively, these results indicate that the nonadjacent energy transfer proceeds via a

[†] Washington University.
[§] Present address: Department of Chemistry, University of Wisconsin, Madison, WI 53706.
[‡] University of Rochester.
[¶] North Carolina State University.
[#] University of California.

10.1021/jp047803j CCC: $27.50
Published on Web 08/03/2004

CHART 1

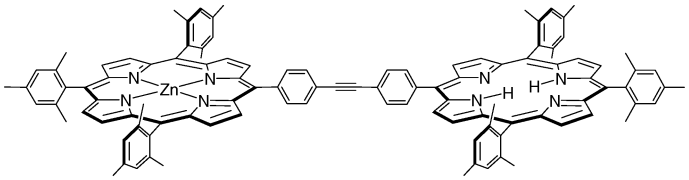

Zn^{U}Fb 24 ± 2 ps

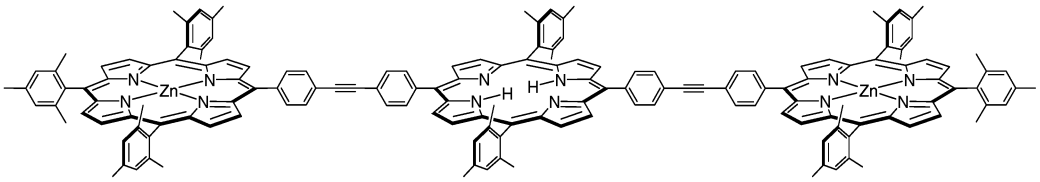

Zn^{U}Fb^{U}Zn 22 ± 3 ps

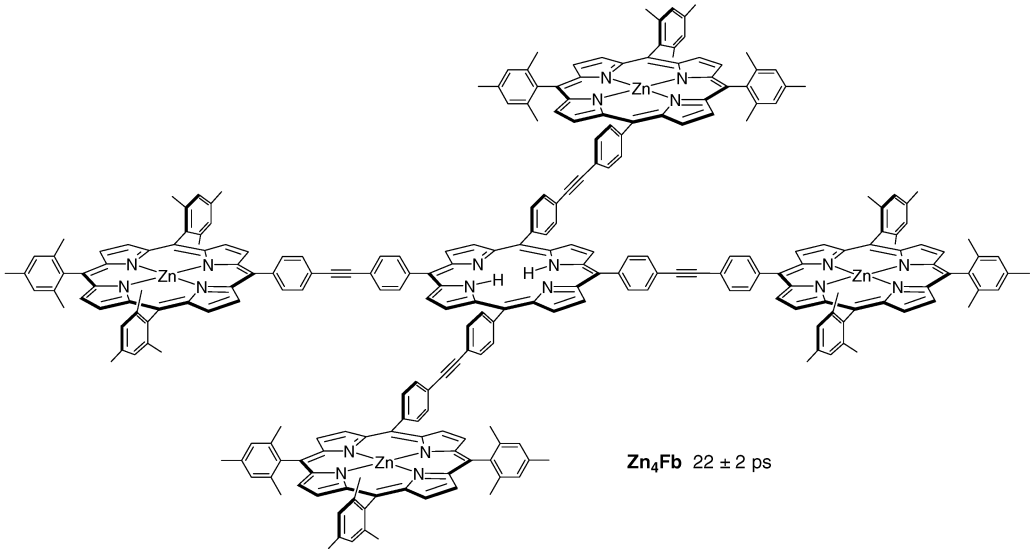

Zn$_4$Fb 22 ± 2 ps

CHART 2

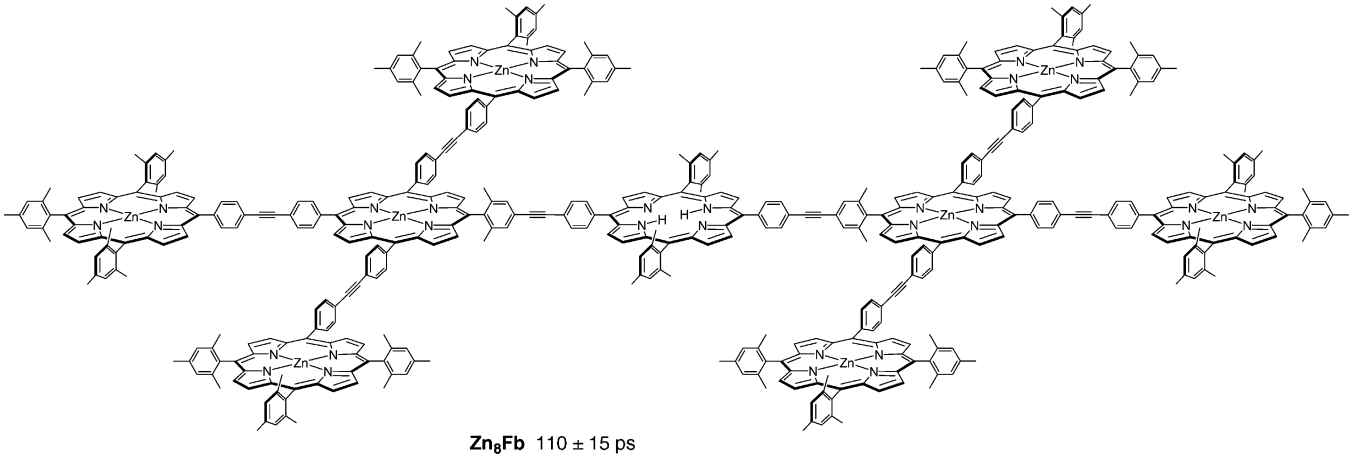

Zn$_8$Fb 110 ± 15 ps

superexchange pathway that uses the intervening zinc porphyrin as the mediator. A two-step mechanism is not viable, especially at low temperatures, because a discrete Zn* excited-state intermediate is energetically far uphill. In triads in which the magnesium porphyrin is chemically or electrochemically oxidized, nonadjacent transfer occurs in the opposite direction from the free base porphyrin to the magnesium porphyrin π cation because the porphyrin π cation is a nonradiative energy sink.[17]

The studies of **Mg^{U}Zn^{U}Fb** and other MgZnFb porphyrin triads have shown that the energy-transfer rates between nonadjacent porphyrins are within an order of magnitude of those between adjacent porphyrins.[17] The relatively small difference in the rates of these two processes implies that nonadjacent transfer has a significant effect on the overall rate and efficiency of energy flow to the lowest-energy trap site. The importance of the nonadjacent energy-transfer pathway should be amplified in large light-harvesting systems and in long molecular wires that contain many identical chromophores. In these systems, bidirectional transfers between adjacent identical chromophores causes a particular site to be revisited

CHART 3

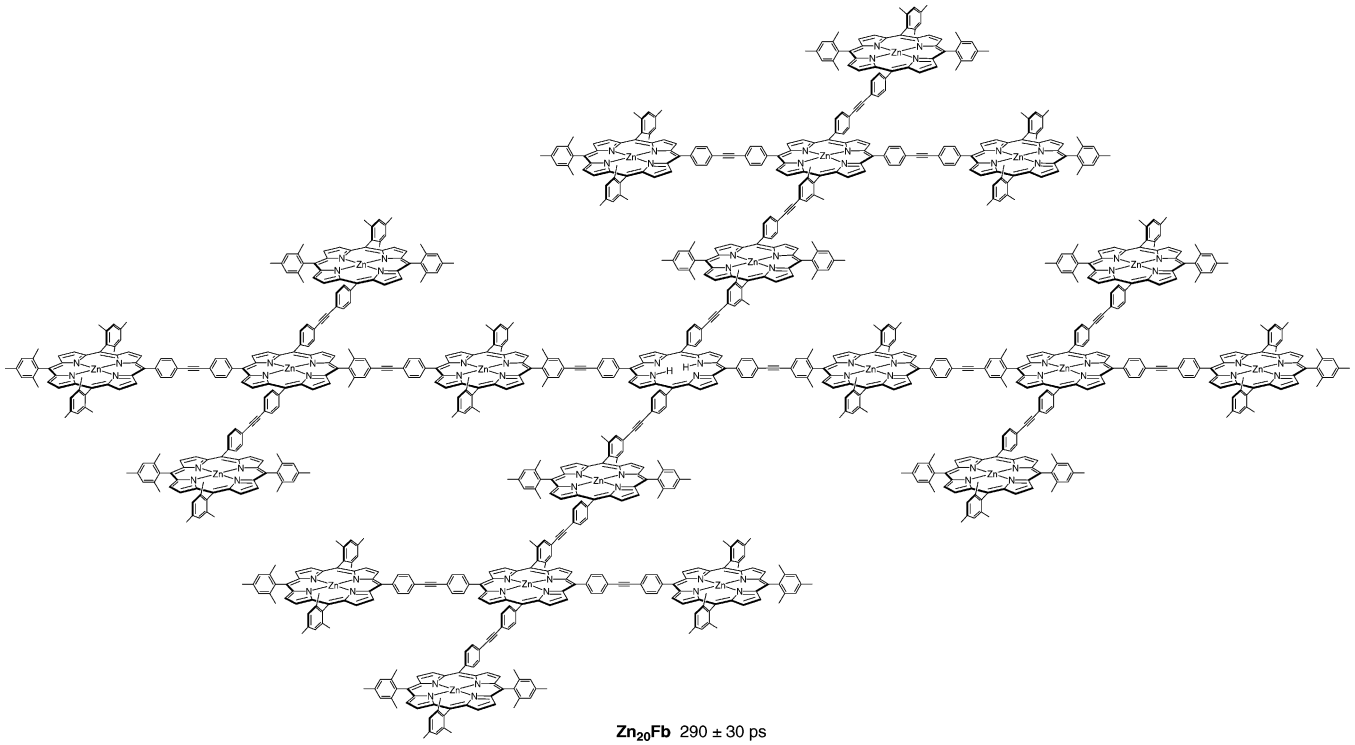

$Zn_{20}Fb$ 290 ± 30 ps

CHART 4

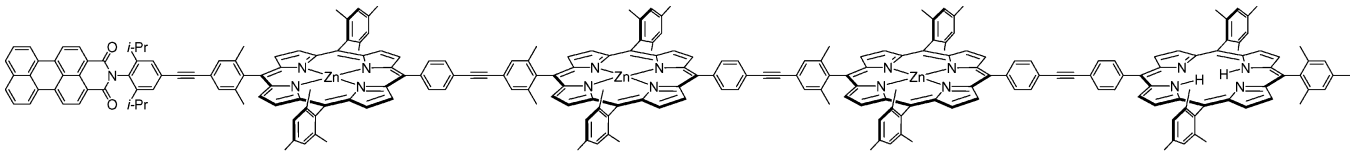

wire 1 170 ± 30 ps

CHART 5

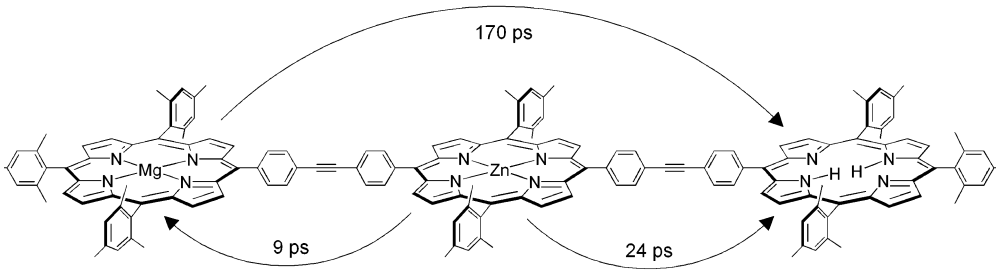

$Mg^{U}Zn^{U}Fb$

many times in the overall energy-transfer cascade; at each visitation the probability of nonadjacent transfer is extant.

The full impact of the nonadjacent transfer process on energy flow in large multiporphyrin arrays such as those shown in Charts 2−4 has yet to be elucidated. Further investigation of this process in these arrays requires knowledge of the rates of all transfer processes between adjacent chromophores. In the case of nonidentical chromophores, the unidirectional energy-transfer rates are readily accessible via the distinct spectroscopic signatures of the donor and acceptor molecules[18] (e.g., from porphyrin dyads such as those shown in Chart 6).[3] On the other hand, the experimental determination of the rate of energy transfer between nominally identical chromophores is elusive because of the lack of a straightforward spectroscopic handle for this type of intersite energy-transfer process (e.g., for pairs of zinc porphyrins in the arrays shown in Charts 2−4). Anisotropy measurements (involving either absorption or fluorescence probing) can, in principle, provide access to transfer processes involving identical chromophores. However, the interpretation of these data can be complicated if exciton coupling is significant.[19]

Early studies of a ZnZnFb triad indicated a value of ∼(50 ps)$^{-1}$ for the rate of bidirectional energy transfer between the diarylethyne-linked zinc porphyrins (denoted Zn ↔ Zn).[20] This value also accounts for the rate of energy flow in a multiporphyrin array linked to a fullerene.[21] Studies of nonadjacent zinc porphyrins that are cofacially, noncovalently stacked in films[22] or joined by multiple phenyl-ethynyl linkers[23] have derived energy-transfer rates of ∼(200 ps)$^{-1}$. The porphyrin−porphyrin electronic interactions in these systems are quite different from each other and from those in the diarylethyne-linked arrays that we have been investigating. To ensure the accuracy of the Zn

CHART 6

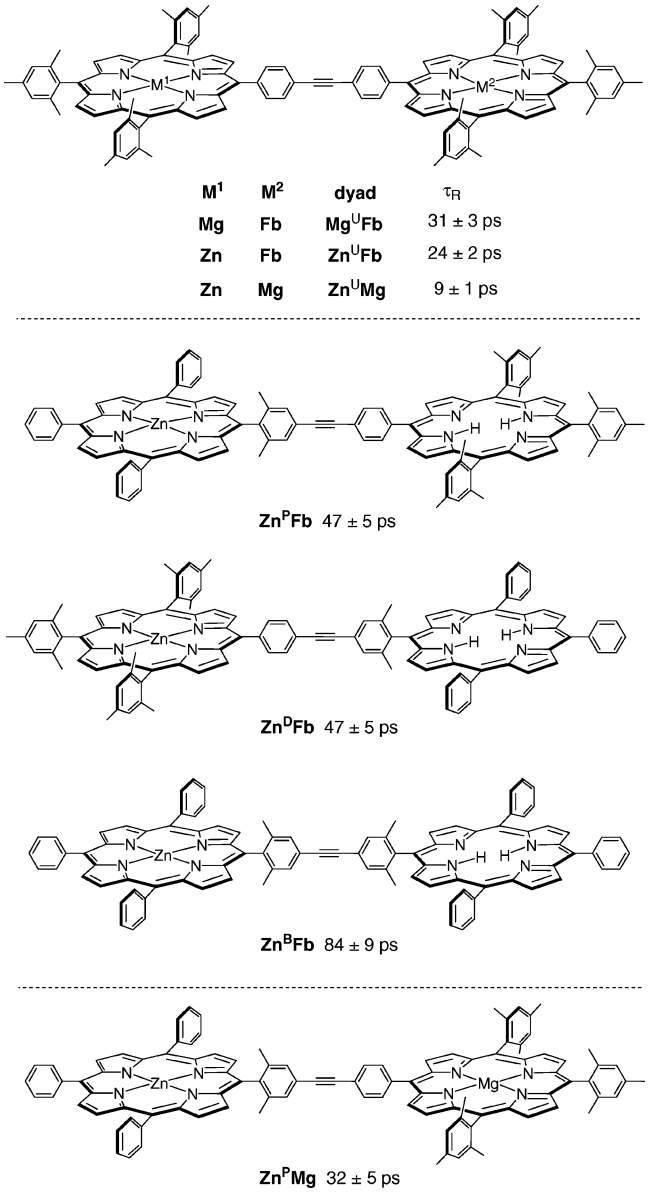

↔ Zn rate for a given structural motif (e.g., linker and connection sites), a more in-depth analysis that incorporates this motif in multiple arrays with different overall architectures is required.

The considerations noted above prompted us to undertake a detailed study aimed at probing (1) the contribution of energy transfer between nonadjacent pigments in multiporphyrin arrays, (2) the rate of bidirectional energy transfer between nominally identical zinc porphyrins, and (3) the dependence of these two processes on porphyrin-linker characteristics. This investigation involved iterative cycles of molecular design, synthesis, determination of energy-transfer rates via ultrafast transient absorption spectroscopy, and kinetic modeling. The study allowed us to set windows on the rate constant for the site-to-site energy transfer between zinc porphyrins with different diarylethyne linkers and to demonstrate unequivocally the necessity of including energy transfer between nonadjacent sites to account for the photodynamics of multichromophore arrays.

Strategy

Our strategy for assessing the rates of nonadjacent and bidirectional energy transfer entailed the following: (1) examining the photodynamics of a family of multiporphyrin arrays, where each array is composed of one or more metalloporphyrins and one low-energy trap; (2) modulating the bidirectional Zn ↔ Zn rate via the degree of steric hindrance on the linker; (3) modulating the unidirectional Zn → trap rate by a combination of steric hindrance on the linker and the use of a free base or magnesium porphyrin as the trap (Zn → Fb or Zn → Mg); and (4) determining the dependence of τ_R (rise of energy at the trap) on the relative rates of the Zn ↔ Zn process and the culminating Zn → trap process across the series of arrays. Through the use of molecular design and chemical synthesis, we could alter which of the two processes is rate-limiting in the overall energy-transfer cascade and thereby refine the assessment of the Zn ↔ Zn rate. The refining of the Zn ↔ Zn rate proceeded in parallel with the analysis of the nonadjacent transfer process to produce a "best" value for the rate of each type of process.

The study required the characterization of the energy-transfer dynamics of a large number of multiporphyrin architectures. The data were obtained in part from our prior work on the large architectures shown in Charts 1−5 complemented with the dyads, triads, and hexad shown in Charts 6−8, respectively. Most of the molecules were available previously, including dyads (**Zn^{U}Fb**,[12] **Zn^{P}Fb**,[12] **Zn^{D}Fb**,[12] **Zn^{B}Fb**,[12] **Zn^{U}Mg**,[24] and **Mg^{U}Fb**[14]), triads (**Zn^{U}Fb^{U}Zn**,[13] **Zn^{U}Zn^{U}Fb**,[25] **Zn^{D}Zn^{U}Fb**,[16] **Zn^{U}Zn^{P}Fb**,[12] and **Mg^{U}Zn^{U}Fb**[25]), and larger arrays (**wire 1**,[16] **Zn$_4$Fb**,[14] **Zn$_8$Fb**,[15] and **Zn$_{20}$Fb**[15]). In addition to arrays connected by an unhindered linker (**U**), this series includes arrays in which *o*,*o*′-dimethyl steric constraints are present on the aryl ring of the linker that is proximal (**P**) or distal (**D**) to the porphyrin that is post-superscripted or arrays in which steric constraints are present on both (**B**) aryl rings of the linker. Implementation of our strategy required the synthesis of five new arrays, including a dyad (**Zn^{P}Mg**), several triads (**Zn^{U}-Zn^{U}Mg**, **Zn^{U}Zn^{P}Mg**, and **Zn^{D}Zn^{U}Mg**), and a hexad (**Zn$_5$Fb**). The syntheses are described in the Supporting Information.

For each new array and several not studied previously, ultrafast transient absorption spectroscopy (of samples in toluene at room temperature) was used to determine the τ_R value following the excitation of a zinc porphyrin constituent with a 130-fs flash. In each case, the growth of bleaching of the ground-state absorption of the trap porphyrin, decay of the zinc porphyrin bleaching, and evolution of the excited-state absorption were generally well described by a single exponential function with the same time constant τ_R within experimental error. These molecules and τ_R values are **Zn^{P}Mg** (32 ± 5 ps), **Zn^{U}Fb^{U}Zn** (22 ± 3 ps), **Zn^{U}Zn^{U}Fb** (55 ± 10 ps), **Zn^{D}Zn^{U}Fb** (60 ± 10 ps), **Zn^{U}Zn^{U}Mg** (20 ± 5 ps), **Zn^{U}Zn^{P}Mg** (55 ± 10 ps), **Zn^{D}Zn^{U}Mg** (30 ± 5 ps), and **Zn$_5$Fb** (320 ± 30 ps). The transient absorption studies on these arrays and several investigated previously are described in the Supporting Information.

A key component of our strategy is the knowledge of pairwise energy-transfer rates determined from a family of porphyrin dyads (Chart 6). The four ZnFb dyads show how energy transfer between zinc and free base porphyrins depends on the steric hindrance on the linker aryl rings.[12] Steric hindrance either proximal to the zinc porphyrin (**Zn^{P}Fb**) or distal (**Zn^{D}Fb**) causes a 2-fold reduction in the energy-transfer rate to $(47\ \text{ps})^{-1}$ from $(24\ \text{ps})^{-1}$ for the unhindered linker (**Zn^{U}Fb**). The investigation also made use of the prior results concerning the dependence of the interporphyrin energy-transfer rate on the nature of the central metal ions.[24] Of particular interest is the increase in the energy-transfer rate to $(9\ \text{ps})^{-1}$ in **Zn^{U}Mg** from $(24\ \text{ps})^{-1}$ in **Zn^{U}Fb**. As with the ZnFb dyads, the introduction of steric

CHART 7

Chart 7

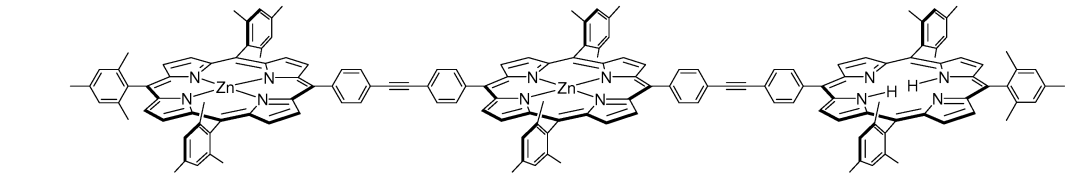

$Zn^{U}Zn^{U}Fb$ 55 ± 10 ps

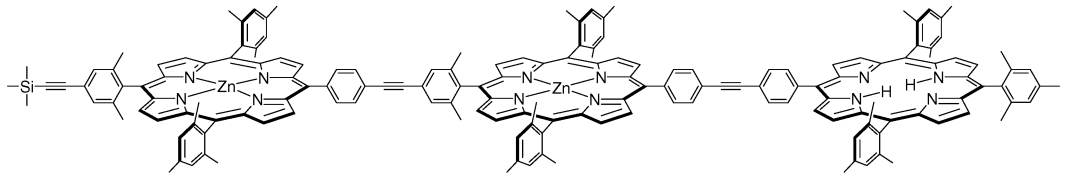

$Zn^{D}Zn^{U}Fb$ 60 ± 10 ps

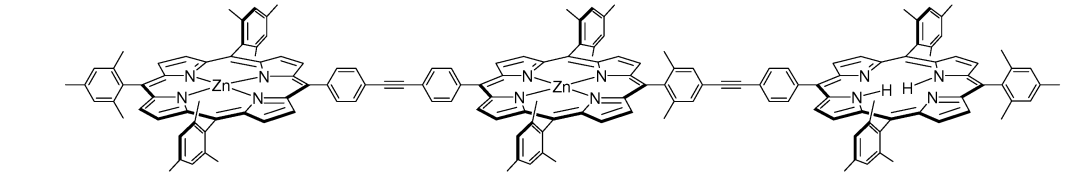

$Zn^{U}Zn^{P}Fb$ 90 ± 10 ps

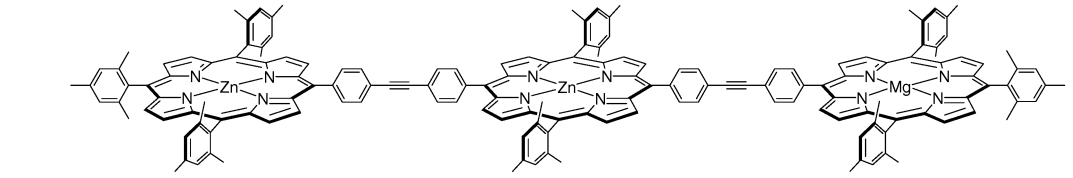

$Zn^{U}Zn^{U}Mg$ 20 ± 5 ps

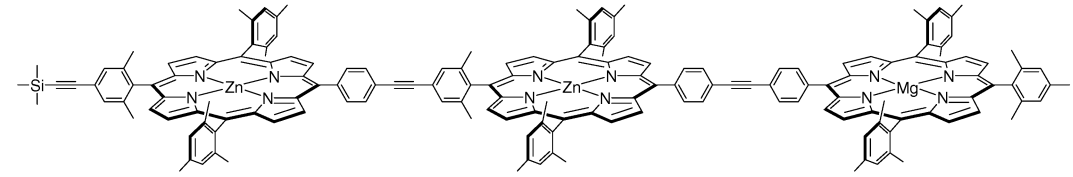

$Zn^{D}Zn^{U}Mg$ 30 ± 5 ps

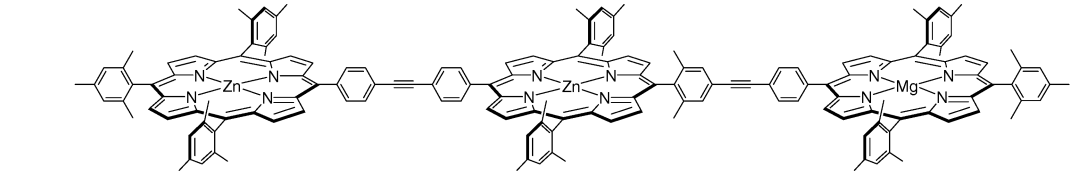

$Zn^{U}Zn^{P}Mg$ 55 ± 10 ps

hindrance causes the energy-transfer rate for **$Zn^{P}Mg$** to slow to $(32\ \text{ps})^{-1}$.

The six triads shown in Chart 7 were essential for implementing our strategy because triads represent the smallest array in which most of the dynamic processes of interest can occur: bidirectional energy transfer between isoenergetic zinc porphyrins, unidirectional energy transfer to a low-energy trap, and unidirectional energy transfer between nonadjacent porphyrins. The triads also incorporate structural features for the modulation of the rates similar to those of the dyads, including unhindered or hindered linkers and a free base or magnesium porphyrin as the low-energy trap. The large dendrimeric arrays **Zn_8Fb** and **$Zn_{20}Fb$** (Charts 2 and 3, respectively) can exhibit one dynamic process that is not present in the triads: bidirectional transfer between nonadjacent zinc porphyrins. The new array **Zn_5Fb** represents one arm of the **$Zn_{20}Fb$** array and provides a valuable cross-check on our observations of the latter architecture (Chart 8). The energy-transfer times for the triads were combined with the results on the larger arrays and subjected to extensive kinetic modeling.

Kinetic Analysis: General Considerations

Methods and Rationale. Analysis of the kinetic data involved both simulations of the observed τ_R values for a given

CHART 8

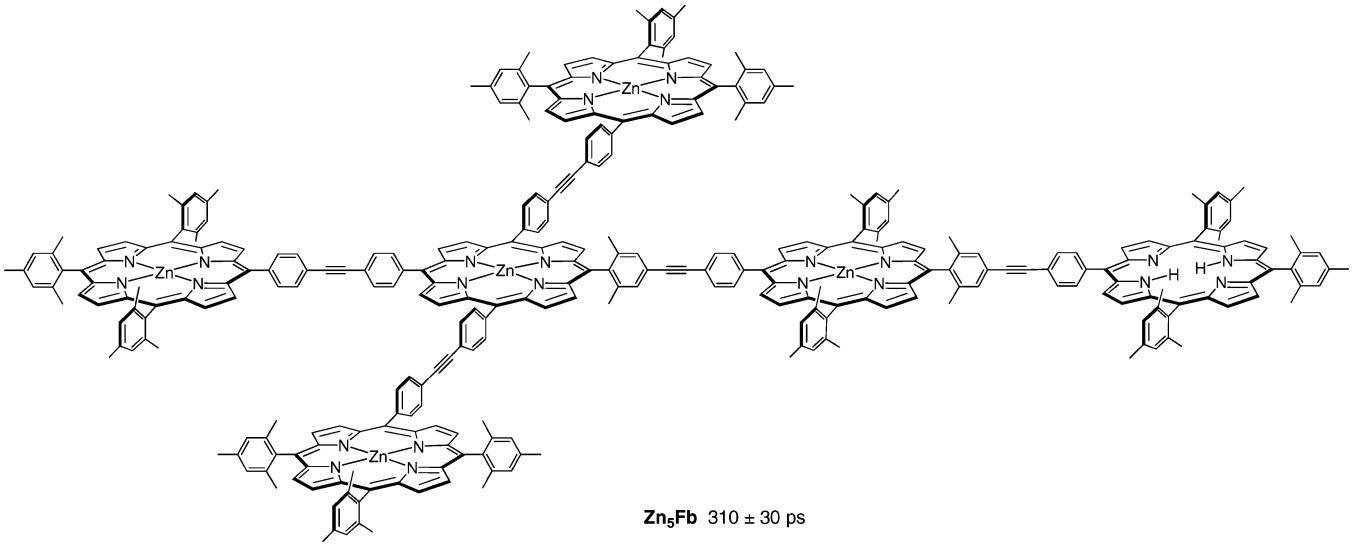

complex and global fitting of the entire data set. The analysis is based on the broad assumption that excitations in the structures under consideration can be treated as localized and that the symmetries of the structures allow a reasonable restriction of the number of fitting parameters. A detailed discussion of the rationale of the theory is given in Appendix 1.

Individual simulations were carried out using the appropriate kinetic equations evaluated using both the KINSIM[26] program and kinetic eigenvalue routines written in MATLAB. These simulations provided insights into the ranges of parameters that would reproduce the observed τ_R values within experimental uncertainty. In the global-fitting procedure, the rate constants obtained from the individual simulations were used as initial guesses for the input into the MATLAB simplex fitting routine "fmins". This routine was used to minimize the squared deviations of the calculated τ_R values for nine arrays (six triads, a wire, the nonamer, and the 21-mer) from the experimental target values with certain constraints.

The KINSIM routine solves the kinetic equations by numerical integration using input values for the rate constants of the individual processes and initial populations. The routine returns the rise of the trap population with time, which is then fit with a function consisting of a constant and a single exponential with time constant τ_R. The fact that the experimental data are well-fit by a single exponential function (as seen from the kinetic profiles given in the Supporting Information) indicates that multiexponential fits are not justified. Thus, the simulated population rise at the trap for each array was analyzed in exactly the same manner as the experimental data. These simulations give initial insights into the intrinsic rate constants for the various energy-transfer processes (e.g., for Zn ↔ Zn transfer and nonadjacent transfer). However, a broad range of values for the rate constants can generally reproduce the experimental τ_R value for any given array. To narrow the range for the Zn ↔ Zn transfer rate with and without steric hindrance in the linker, sets of rate constants were used to obtain the τ_R values for several different arrays. Comparisons were made to seek consistency in the rate constants for common processes while reproducing all of the τ_R values within the experimental error bars. More calculations were performed as necessary wherein additional arrays were incorporated in the manual analysis, the cycle was restarted, and so on. Although this procedure is useful for the initial assessment of the acceptable parameter space, it is laborious and not as comprehensive as the automated global analysis of the entire data set.

The approach using MATLAB routines is superior for several reasons. First, the method directly returns kinetic eigenvalues. These eigenvalues are functions of the rate constants of the individual processes and, as such, represent characteristic times of the kinetic system. The eigenvalues and their eigenvectors together enable exact solutions to the kinetic equations and, thus, can be used to generate the population evolution at the trap (just as with KINSIM). Second, the eigenvalue approach provides the means for implementing the global analysis. This is so because one of the kinetic eigenvalues overwhelmingly dominates in describing the τ_R value for each system studied here. Thus, the large parameter space spanned by the intrinsic rate constants could be sampled, the calculated dominant eigenvalue for each array continually compared with the measured τ_R value (and the experimental error bar), and any differences minimized in parallel for all of the arrays.

The two methods (global analysis using the dominant eigenvalues and fits of the individual simulations) have one difference that is worthy of comment. In particular, for the largest arrays (**wire 1**, **Zn_8Fb**, and **Zn_{21}Fb**), the inverse of the dominant rate eigenvalue is 15−20% smaller than the rise time obtained by fitting the entire calculated population rise at the trap to an unconstrained single exponential function. For smaller arrays such as the triads, this difference is less than 10%. These differences arise because the other (larger) eigenvalues, corresponding to smaller time constants, also contribute to the dynamics. This contribution is primarily due to the very earliest stages of the dynamics for the systems studied here because their amplitude is preferentially weighted from the excitations initially residing on the zinc porphyrins closest to the trap. However, any differences in assessing the τ_R values using the dominant eigenvalue from global analysis or fits to the complete calculated population kinetics from individual simulations are within the experimental error. Thus, the two methods are complementary and reinforcing in providing access to the intrinsic rate constants. The intrinsic rate constants are fundamental to the kinetic system and can be used to make predictions about the dynamics of next-generation multiporphyrin arrays.

Kinetic Equations. In the initial kinetic modeling, the analysis included the energy transfer only between adjacent pigments. Figure 1A introduces these kinetic pathways for the case of a triad containing two zinc porphyrins and a low-energy

trapping site that may be either a magnesium porphyrin or a free base porphyrin. As is the case for all six triads studied here, the rate constant K_{trap} for the unidirectional transfer of excitation energy to the trap has been determined from studies of the appropriate dyad containing the same trap porphyrin and the same steric hindrance in the linker (Chart 6). In the case of the triads, a τ_R value longer than $1/K_{trap}$ is expected (and observed) because of the presence of the zinc porphyrin distant from the trap and the reversible Zn ↔ Zn transfer process.

The simplest kinetics for the case of the triad depicted in Figure 1A may be written

$$\frac{dP_1(t)}{dt} = -k^0_{trap}P_1(t) + K_{trap}P_2(t)$$

$$\frac{dP_2(t)}{dt} = -(k^0_{Zn} + K_{trap} + K_{ZnZn})P_2(t) + K_{ZnZn}P_3(t) + I_2(t) \quad (1)$$

$$\frac{dP_3(t)}{dt} = K_{ZnZn}P_2(t) - (k^0_{Zn} + K_{ZnZn})P_3(t) + I_3(t)$$

where $P_n(t)$ is the relative probability that excitation is on chromophore n, $I_n(t)$ is the relative rate of excitation of chromophore n, and k^0_{Zn} and k^0_{trap} are the rates of decay of the excited zinc porphyrin and the trap porphyrin, respectively, in the absence of excitation transfer. If the excitation pulse is short compared with all characteristic times, the excitation terms $I_n(t)$ may be removed and replaced by using the initial conditions $P_n(0)$. Given that the singlet excited-state lifetimes of zinc, magnesium, and free base porphyrin reference monomers are approximately 2, 10, and 13 ns, respectively,[27] and the rate of energy transfer in typical diarylethyne-linked porphyrin dyads is $>(100\ ps)^{-1}$ (Chart 6), the monomer decay terms k^0_{trap} and k^0_{Zn} are small compared with K_{ZnZn} and K_{trap}. The characteristic times of the system are the eigenvalues of the kinetic matrix

$$\begin{pmatrix} k^0_{trap} & -K_{trap} & 0 \\ 0 & k^0_{Zn} + K_{ZnZn} + K_{trap} & -K_{ZnZn} \\ 0 & -K_{ZnZn} & k^0_{Zn} + K_{ZnZn} \end{pmatrix} \quad (2)$$

which are

$$\lambda = k^0_{trap},\ k^0_{Zn} + K_{ZnZn} + \frac{1}{2}K_{trap} \pm \sqrt{\frac{1}{4}(K_{trap})^2 + (K_{ZnZn})^2} \quad (3)$$

The eigenvalue containing the negative square root term is the one of principal interest because it is dominant in determining the main component of the rise of excitation on the trap (τ_R). This eigenvalue has the smallest value and, thus, represents the smallest rate and largest τ_R (other than the trap's intrinsic decay rate).

Preliminary Estimates of Key Rates. Figure 2 shows the results of a test of the kinetic relation for four triads having different trapping time constants ($1/K_{trap}$) and measured rise times (τ_R) as follows: 47 and 90 ps for **Zn^{U}Zn^{P}Fb**, 32 and 55 ps for **Zn^{U}Zn^{P}Mg**, 24 and 55 ps for **Zn^{U}Zn^{U}Fb**, and 9 and 20 ps for **Zn^{U}Zn^{U}Mg**, respectively. If the simple model described above were applicable, τ_R values would be predicted to lie at the intersections of a vertical line with the four curves at the value $1/K_{ZnZn}$ for the Zn ↔ Zn energy transfer. However, it is clear from the most cursory inspection that only two cases can be explained at all: for **Zn^{U}Zn^{U}Mg** the required $1/K_{ZnZn}$ is about 4 ps, and for **Zn^{U}Zn^{U}Fb** the requirement is $1/K_{ZnZn} = 16$ ps. For **Zn^{U}Zn^{P}Fb**, a $1/K_{ZnZn}$ value of <1 ps might predict a rise time that agrees with the observation within measurement errors, but for **Zn^{U}Zn^{P}Mg**, there is no fit at all.

We next amended the simple model described above by including the energy transfer between nonadjacent pigments, a process that we know is operative in triads from our previous studies on **Mg^{U}Zn^{U}Fb** (Chart 5). Figure 1B introduces this kinetic pathway. Here, L is the rate constant for the unidirectional transfer from the distal zinc porphyrin to the nonadjacent trap porphyrin, and K is the rate for the adjacent transfers. In larger arrays, M is the rate for the nonadjacent transfers involving only zinc porphyrins (note that there are different values for each of L, M, and K, depending on the combination of porphyrin and linker steric hindrance). The addition of nonadjacent energy transfer modifies the kinetic matrix to

$$\begin{pmatrix} k^0_{trap} & -K_{trap} & -L \\ 0 & k^0_{Zn} + K_{ZnZn} + K_{trap} & -K_{ZnZn} \\ 0 & -K_{ZnZn} & k^0_{Zn} + K_{ZnZn} + L \end{pmatrix} \quad (4)$$

with a corresponding complication in the eigenvalues that will not be detailed here.

With the introduction of nonadjacent energy transfer, the observed rise times for the four triads with the same unhindered linker between zinc porphyrins (**Zn^{U}Zn^{U}Mg**, **Zn^{U}Zn^{U}Fb**, **Zn^{U}Zn^{P}Mg**, and **Zn^{U}Zn^{P}Fb**) can now be reproduced with a single value of K_{ZnZn}. However, the range of possible values of $1/K_{ZnZn}$ is broad (10−60 ps) if one allows an arbitrary choice of the rate constant L for the nonadjacent energy transfer in each triad. To reduce the span of values, it is necessary to evaluate what one might expect for the nonadjacent energy-transfer rates in the different triads and to incorporate the other arrays in the analysis.

In Appendix 2, we estimate the nonadjacent energy-transfer rates using our measured value of $L = (170\ ps)^{-1}$ in **Mg^{U}Zn^{U}Fb** as a starting point. This rate is scaled using the rates of transfer between adjacent porphyrins in the dyads containing the same donor and acceptor porphyrins and steric hindrance (Chart 6). The estimated rates are $\sim(130\ ps)^{-1}$ for **Zn^{U}Zn^{U}Fb**, $(250\ ps)^{-1}$ for **Zn^{U}Zn^{P}Fb**, $(50\ ps)^{-1}$ for **Zn^{U}Zn^{U}Mg**, and $(180\ ps)^{-1}$ for **Zn^{U}Zn^{P}Mg**. Despite the limitations of the simple scaling method used, the values obtained for nonadjacent energy transfer were found to be useful for the initial screening of the individual kinetic simulations. Moreover, these values were ultimately found to be consistent with those deduced from the global fits of the energy-transfer dynamics in the arrays.

Kinetic Analysis: Determination of the Rate Constants

Analysis for Individual Arrays. From calculations using the appropriate kinetic equations, we obtained the τ_R value for each of the triads and larger arrays as a function of the appropriate rate constants (K, L, and M). The results of some individual simulations on the six triads (Chart 7) are tabulated in the Supporting Information. Also given there are the associated contour plots showing the dependence of the τ_R on (1) the rate constant L of unidirectional energy transfer between nonadjacent porphyrins and (2) the rate constant K_{ZnZn} of bidirectional energy transfer between adjacent zinc porphyrins. In Appendix 3, we describe some of the results for triads **Zn^{U}Zn^{U}Mg** and **Zn^{D}Zn^{U}Mg** to convey the logic employed in the analysis. A contour plot that covers the parameter ranges for these two arrays is shown in Figure 3. These two triads were chosen because they incorporate the **Zn^{U}Mg** dyad motif, which exhibits the fastest unidirectional energy-transfer rate among all of the

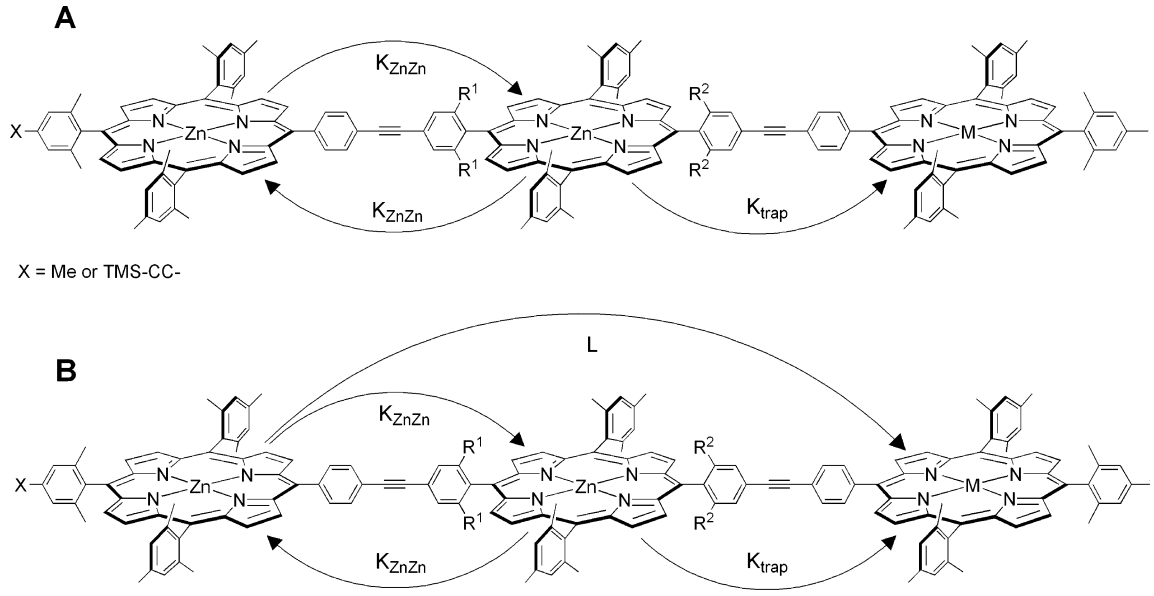

Triad	M	R^1	R^2	$(K_{trap})^{-1}$ (ps)	τ_R (ps)
Zn^UZn^UFb	H,H	H	H	24	55 ± 10
Zn^UZn^PFb	H,H	H	Me	47	90 ± 10
Zn^DZn^UFb	H,H	Me	H	24	60 ± 10
Zn^UZn^UMg	Mg	H	Me	9	20 ± 5
Zn^UZn^PMg	Mg	H	Me	32	55 ± 10
Zn^DZn^UMg	Mg	Me	H	9	30 ± 5

Figure 1. Kinetic models for the triads without (A) and with (B) nonadjacent energy transfer.

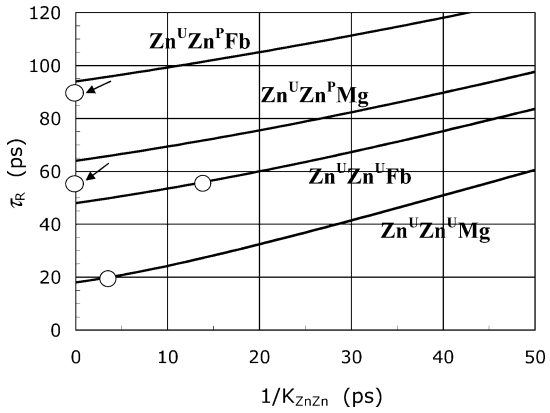

Figure 2. Values of the rise time τ_R of the energy on the trap porphyrin as a function of the inverse of the rate constant K_{ZnZn} of reversible energy transfer between zinc porphyrins in triads (as predicted by the model shown in Figure 1A). The model does not incorporate energy transfer between the nonadjacent zinc and trap porphyrins.

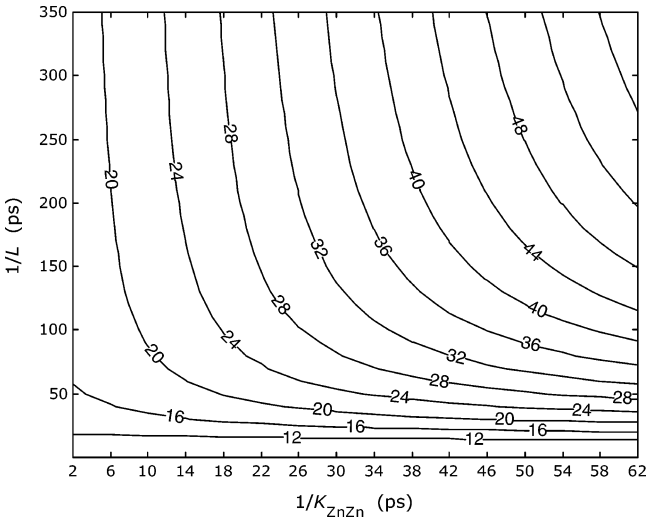

Figure 3. Contour plot for triads **Zn^UZn^UMg** and **Zn^DZn^UMg**, showing the dependence of the rise time τ_R of the energy transfer to the Mg porphyrin on the inverse of the rate constant L (for the unidirectional energy transfer between nonadjacent Zn and Mg porphyrins; ordinate) and the inverse of the rate constant K_{ZnZn} (for reversible energy transfer between Zn porphyrins; abscissa). These calculations employed a rate constant $K_{trap} = (9\ \text{ps})^{-1}$ for the trapping process involving adjacent zinc and magnesium porphyrins.

arrays examined. The high rate of the trapping step enables the initial tightening of the window on the Zn ↔ Zn transfer rate to $1/K_{ZnZn} = 10-35$ ps with no steric hindrance (as in **Zn^UZn^UMg**) and $1/K_{ZnZn} = 30-55$ ps with steric hindrance (as in **Zn^DZn^UMg**). The latter value is further narrowed to a 35−55 ps range when combined with the results of **wire 1** (Chart 4), in which the two linkers joining the three zinc porphyrins are sterically hindered. Furthermore, the values for $1/K_{ZnZn}$ in **Zn^UZn^UMg** and **Zn^DZn^UMg** occur for values for the nonadjacent transfer ($1/L$ in the ranges of 50−100 and 70−350 ps, respectively) that are reasonable on the basis of the estimates obtained above using the known value for **Mg^UZn^UFb** as a reference.

The fact that the values of L for the nonadjacent transfer are typically within a factor of 5−10 of those of the adjacent transfer

has important consequences for the properties of the triads and larger arrays. The efficacy of the nonadjacent transfer process underlies the observation that τ_R increases in the triads only marginally when steric hindrance is added between zinc porphyrins, namely, from 20 ± 5 ps in **Zn^{U}Zn^{U}Mg** to 30 ± 5 ps in **Zn^{D}Zn^{U}Mg** and from 55 ± 10 ps in **Zn^{U}Zn^{U}Fb** to 60 ± 10 ps in **Zn^{D}Zn^{U}Fb**. This "diluted" steric-hindrance effect on the overall energy transfer from that for K_{ZnZn} alone is physically reasonable when one considers that the nonadjacent energy-transfer process provides a bypass for the Zn ↔ Zn energy-transfer equilibrium in the triads (Figure 1). Additionally, the **Zn$_8$Fb** nonamer (Chart 2) demands inclusion of the nonadjacent transfer in the kinetic modeling. Without the nonadjacent transfer ($L = 0$), a value for $1/K_{ZnZn}$ even as small as 2 ps (which is below the acceptable range for many arrays) affords τ_R only as small as ∼180 ps, which is far larger than the observed value of 110 ± 15 ps. If on the other hand, nonadjacent transfers are given values $1/L > 100$ ps, which are reasonable on the basis of the estimates given above, then the observed energy arrival times are reproduced with $1/K_{ZnZn}$ values in the range of those described above for the triads, namely, 10−35 ps without steric hindrance and 35−55 ps with steric hindrance.

Global Fits for Multiple Arrays. To obtain a comprehensive assessment of the energy-transfer dynamics, we simultaneously minimized the squared deviations of the τ_R values for nine arrays, namely, the triads (**Zn^{U}Zn^{U}Mg**, **Zn^{D}Zn^{U}Mg**, **Zn^{U}Zn^{P}Mg**, **Zn^{U}Zn^{U}Fb**, **Zn^{D}Zn^{U}Fb**, and **Zn^{U}Zn^{P}Fb**), **wire 1**, and the dendrimers **Zn$_8$Fb** and **Zn$_{20}$Fb**. The parameters derived from the analysis of the individual simulations were used as inputs for the global analysis. Numerous fits were performed using various constraints on the parameters. The principal (and experimentally justified) constraint is that steric hindrance slows the energy transfer between either adjacent or nonadjacent pigments. When this restriction was implemented, the rates changed little when other constraints were added. For example, in the fitting that results in the parameters presented in Tables 1 and 2, a second constraint was that the nonadjacent transfer rate between porphyrins in a right-angle (90°) arrangement in the dendrimeric arrays has a rate that is the same as that for an in-line (180°) configuration (Charts 2 and 3). When the second constraint is relaxed, the Zn ↔ Zn transfer rates (with and without steric hindrance) do not change appreciably, and the nonadjacent transfer rates for the 90 and 180° configurations for a given motif (porphyrins and steric hindrance) are within a factor of 2 of one another. The end result of these and other fits, and the analysis of the individual simulations, is that the rate of energy transfer between adjacent zinc porphyrins is 30 ± 10 ps (no steric hindrance) or 50 ± 10 ps (with steric hindrance on one of the aryl rings of the linker).

Values of the rate constants M for the nonadjacent transfers involving only Zn porphyrins were not well-determined, owing in part to the processes appearing in a limited number of arrays (**Zn$_8$Fb**, **Zn$_{20}$Fb**, or **wire 1**) along with the excessive number of parameters generated compared to the target values. Therefore, in some global analysis runs, these rate constants were set to 1/(1000 ps), except for M_4, which was set to 1/(2000 ps). In other runs, these rate constants were set to zero. Such values of M did not change any of the other rate constants appreciably from those given in the table, including the rate constants K_1 and K_2 for the Zn ↔ Zn transfer involving adjacent porphyrins (without and with steric hindrance in the linker). The range of M values in **wire 1** and the dendrimeric arrays were investigated in the individual simulations. The experimental τ_R values were well-reproduced with M values on the same order of magnitude as the L values for the nonadjacent transfer involving different porphyrins (mediated by a zinc porphyrin). Improvement in the determination of the M rates requires the synthesis and study of additional arrays, particularly arrays containing long series of zinc porphyrins for which the K values are well known. Several such architectures that build on the current designs and together enable more accurate assessment of the M values are listed in italics in Table 2 along with the predicted rise times.

The rate constants for the energy transfer between adjacent zinc porphyrins (K_1 and K_2) are in keeping with the evaluation of selected individual simulations given above. The rate constants L for the energy transfer between nonadjacent zinc and magnesium or free base porphyrins are typically within a factor of 2 of those predicted by the simple method outlined above, where the one measured nonadjacent transfer rate is scaled using the known rates for the dyads (depending on the combination of porphyrins and linker steric hindrance). This knowledge provides a design tool that should be useful in evaluating the impact of nonadjacent transfer in more complex arrays.

TABLE 1: Representative Fits to the Kinetics of Nine Arrays

rate constant	description[a]	occurrence	(measured rate)$^{-1}$ (ps)[b]	(fit rate)$^{-1}$ (ps)
k^0_{Zn}	Zn* decay	9 arrays	2400[c]	fixed
k^0_{Fb}	Fb* decay	6 arrays	13000[c]	fixed
k^0_{Mg}	Mg* decay	3 arrays	10000[c]	fixed
K_1	**Zn^{U}Zn**	6 arrays		35
K_2	**Zn^{P}Zn**	5 arrays		57
K_3	**Zn^{U}Fb**	**Zn^{U}Zn^{U}Fb**, **Zn^{D}Zn^{U}Fb**, **wire 1**	24 ± 2[d]	24
K_4	**Zn^{P}Fb**	**Zn^{U}Zn^{P}Fb**, **Zn$_8$Fb**, **Zn$_{20}$Fb**	47 ± 5[e]	48
K_5	**Zn^{U}Mg**	**Zn^{U}Zn^{U}Mg**, **Zn^{D}Zn^{U}Mg**	9 ± 1[f]	9
K_6	**Zn^{P}Mg**	**Zn^{U}Zn^{P}Mg**	32 ± 5[g]	32
L_1	**Zn^{U}Zn^{U}Fb**	**Zn^{U}Zn^{U}Fb**		215
L_2	**Zn^{U}Zn^{P}Fb**	**Zn^{U}Zn^{P}Fb**		245
L_2'	**Zn^{U}Zn^{P}Fb** (90°)	**Zn$_8$Fb**		245
L_3	**Zn^{D}Zn^{U}Fb**	**Zn^{D}Zn^{U}Fb**, **wire 1**		225
L_4	**Zn^{D}Zn^{D}Fb**	**Zn$_{20}$Fb**		380
L_5	**Zn^{U}Zn^{U}Mg**	**Zn^{U}Zn^{U}Mg**		40
L_6	**Zn^{U}Zn^{P}Mg**	**Zn^{U}Zn^{P}Mg**		115
L_7	**Zn^{D}Zn^{U}Mg**	**Zn^{D}Zn^{U}Mg**		55
M_1−M_4	**Zn^{U}Zn^{U}Zn**, etc.	**wire 1**, **Zn$_8$Fb**, **Zn$_{20}$Fb**		*h*

[a] The configurations with steric hindrance on the linker are given the same rate regardless of whether the hindrance is located in a proximal (**P**) or distal (**D**) arrangement to a given porphyrin. The configurations with right-angle (90°) configurations of the three porphyrins occur in the dendrimeric arrays (**Zn$_5$Fb**, **Zn$_8$Fb**, and **Zn$_{20}$Fb**). [b] Measured in monomers (k values, inverse of excited-state lifetime) or dyads (K values, inverse of the arrival times τ_R for energy at the trap porphyrins). [c] From ref 27. These are the excited singlet-state lifetimes of the isolated tetraarylporphyrin. [d] From ref 16. [e] From values determined here and refs 12 and 15. [f] From ref 17. [g] This work. [h] Not listed are the values for the rate constants M for the nonadjacent transfer involving only Zn porphyrins, which were not well-determined (see text); for the fit shown, all of the M values were set at (1000 ps)$^{-1}$, except for $M_4 = (2000\ \text{ps})^{-1}$. A few other parameters are required for the predictions shown in Table 2. Their values were taken to be $L_1' = L_1$, $L_5' = L_5$, $L_6' = L_6$, and $L_8 = (170\ \text{ps})^{-1}$, where the L_8 process is for the nonadjacent energy transfer in **Zn^{D}Zn^{D}Mg**.

TABLE 2: Rise Time for the Arrival of Energy on the Trap Porphyrin

array	measured τ_R (ps)	fit τ_R (ps)[a]
Zn^UZn^UFb	55 ± 10	55
Zn^UZn^PFb	90 ± 10[b]	86
Zn^DZn^UFb	60 ± 10	65
Zn^UZn^UMg	20 ± 5	22
Zn^UZn^PMg	55 ± 10	55
Zn^DZn^UMg	30 ± 5	30
Zn_8Fb	110 ± 20	121
$Zn_{20}Fb$, Zn_5Fb	300 ± 30[c]	303
wire 1	170 ± 30	144
predictions		
Zn^DZn^DFb[d]		101
Zn^DZn^DMg		65
$Zn^UZn^UZn^UFb$		111
$Zn^PZn^UZn^UFb$		122
$Zn^UZn^PZn^UFb$		130
$Zn^PZn^PZn^UMg$		93
$Zn_{20}Mg$, Zn_5Mg		219
11-mer		164
$Zn^PZn^PZn^PZn^UFb$		252
$Zn^PZn^PZn^PZn^UMg$		187
$Zn^UZn^PZn^PZn^UFb$		242
$Zn^UZn^PZn^PZn^UMg$		174
Zn_8Mg (nonamer 2)		71
nonamer 3		81
nonamer 4		26

[a] The longest nontrivial lifetime (inverse of the smallest nontrivial eigenvalue of the rate matrix) from the fit in Table 1. [b] From values determined here and in ref 12. [c] From values determined here and in ref 15 for **$Zn_{20}Fb$** and here for **Zn_5Fb**. [d] Arrays in italics are the potential targets for future studies for which the values represent predictions. Specific structures are as follows: **Zn_8Mg**, **$Zn_{20}Mg$**, and **Zn_5Mg**, same as the Fb analogues (Charts 2, 3, and 8, respectively) with Mg substitution; ***11-mer***, same as nonamer **Zn_8Fb** with one additional **Zn^U** at each end of the spine; ***nonamer 3***, same as **Zn_8Fb** with no hindrance between Zn and Fb; ***nonamer 4***, same as ***nonamer 3*** with Mg substituting for Fb.

Conclusions and Outlook

The studies reported herein provide a detailed picture of the dynamics of the energy flow in multiporphyrin architectures. A key observation is that the rate of energy flow to a trap is strongly influenced by both the bidirectional transfer between adjacent identical porphyrins and the unidirectional transfers between nonadjacent porphyrins. The rate of energy flow between adjacent identical zinc porphyrins is qualitatively similar to that between adjacent nonidentical porphyrins (e.g., from a zinc to a free base porphyrin). The rate of energy flow between porphyrins at nonadjacent sites is only 5−10-fold slower. In this regard, a comparable ratio of adjacent and nonadjacent transfer rates was obtained for nonlinked porphyrins in a fundamentally different architecture. Monte Carlo simulations of fluorescence lifetime anisotropy data for nonlinked zinc porphyrins cofacially stacked in films derived a nonadjacent transfer rate of $(200\ \text{ps})^{-1}$ that is ∼8-fold slower than that of $\sim(26\ \text{ps})^{-1}$ for the adjacent transfer.[22] In the latter studies, energy transfer occurs exclusively by the Förster through-space mechanism, whereas energy transfer in our diarylethyne-linked arrays is primarily through-bond.[3] These combined results indicate that nonadjacent transfers have a broad impact on the observed dynamics of organized porphyrins spanning very different arrangements of the chromophores and different underlying mechanisms. Nonadjacent transfers impact the energy-transfer dynamics even in arrays as small as triads and, thus, must be considered in the design of virtually any multiporphyrin architecture.

The observation that the energy transfer between nonadjacent porphyrins significantly influences the overall dynamics of energy trapping has important consequences for the design of large light-harvesting complexes and long molecular wires based on the porphyrin paradigm. In particular, for very large architectures, the bidirectional flow of energy between adjacent identical porphyrins ultimately limits the distance over which the energy can be efficiently transferred to a trap. The participation of nonadjacent transfers can mitigate the losses inherent in the reversible steps. Accordingly, architectures for more efficient energy flow might be designed around modules comprised of small numbers of multiple identical pigments attached to local traps that receive energy via both adjacent and nonadjacent processes. These traps would then pass the energy to the ultimate sink.

Finally, we note that the factors that influence the energy transfer in the multiporphyrin arrays are also most likely important for arrays based on other types of chromophores. These factors should be particularly important for arrays based on pigments that are closely related to porphyrins, such as chlorins, phorbins, phthalocyanines, and bacteriochlorins. This consideration suggests that mixed pigment arrays could be designed that would leverage the best features of downhill energy flow, reversible flow between identical pigments, and irreversible flow between nonadjacent pigments.

Acknowledgment. This research was supported by grants from the Department of Energy (J.S.L.) and the National Science Foundation (REU Grant PHY-02-42483, R.A.F.). We thank Dr. Sung Ik Yang and Dr. Robin K. Lammi for assistance with some of the transient absorption measurements. Mass spectra were obtained at the Mass Spectrometry Laboratory for Biotechnology at North Carolina State University. Partial funding for the NCSU Facility was obtained from the North Carolina Biotechnology Center and the NSF.

Appendix 1

Remarks on the Kinetic Model. Several assumptions are made in the kinetic model. (a) System excitations can be characterized by simple population kinetics of localized excitations. (b) Excitation of one of the sites can be projected onto one state, ignoring vibrations. These first two assumptions imply that coherence density matrix components and exciton effects can be ignored. The next several assumptions result in constraints that effectively reduce the number of fitting parameters. (c) The monomeric decay rates (e.g., k^0_{Zn}) are independent of the structure in which the zinc porphyrin is located; these are fixed at the inverse of the observed monomer excited-state lifetimes. (d) Transfer rates between a given pair of nonidentical porphyrins are independent of the nature of the appended subunits (environment). This hypothesis is supported by observations such as the similarity of the rates of the Zn → Fb transfer in the different arrays shown in Chart 1. (e) In analogy to d, transfer between adjacent zinc porphyrins (Zn ↔ Zn) is independent of environment and is the same in both directions ("reversible"). (f) In analogy to d and e, nonadjacent transfer involving a given trio of porphyrins is independent of the overall architecture (e.g., triad or nonamer), and the transfers involving only zinc porphyrins are reversible. (g) Steric hindrance by an *o*,*o*′-dimethyl substitution on one aryl ring of the diarylethyne linker is assumed to be independent of the directionality. This hypothesis is suggested by the finding that the Zn → Fb transfer is the same in dyads **Zn^PFb** and **Zn^DFb** (Chart 6). Assumptions c−g were rigid and used at all times. We also explored the

following concept. (h) Nonadjacent transfer involving a given trio of porphyrins has the same rate whether in a 180° in-line arrangement (as occurs in the triads) or a 90° right-angle configuration (as occurs in the dendrimeric arrays in addition to the in-line configuration). This hypothesis is supported by our finding[3] that the energy transfer in diarylethyne-linked arrays is primarily through-bond in character (and thus minimally dependent on through-space orientation factors) and by the similarity of porphyrin orbital coefficients[28] on adjacent and opposite meso positions (i.e., for the intervening zinc porphyrin).

Appendix 2

Initial Estimates for the Rates of Nonadjacent Energy Transfer. The measured rate constant of $(170\ \text{ps})^{-1}$ for the nonadjacent energy transfer from a magnesium to free base porphyrin (with an intervening zinc porphyrin) in **Mg^{U}Zn^{U}Fb** (Chart 5) is used as a starting point to obtain initial estimates for the other triads. This reference value is scaled using the rates of the energy transfer between adjacent porphyrins in the dyads containing the same donor and acceptor porphyrins (Chart 6). For example, the nonadjacent transfer rate for **Zn^{U}Zn^{U}Fb** is estimated by multiplying the value 170 ps for **Mg^{U}Zn^{U}Fb** by a factor of 24/31 to account for differences in the rate of the trapping step, namely $(24\ \text{ps})^{-1}$ for **Zn^{U}Fb** versus $(31\ \text{ps})^{-1}$ for **Mg^{U}Fb**. The resulting value for **Zn^{U}Zn^{U}Fb** is $1/L_1 \sim 130$ ps. (See Tables 1 and 2 for a summary of the various L values, as well as the K and M values.) Similarly, using the **Zn^{U}Zn^{U}Fb** estimate, the value for **Zn^{U}Zn^{U}Mg** is $1/L_5 \sim (9/24)(130\ \text{ps}) \sim 50$ ps. Using these values and taking into account the effect of steric hindrance in dyads (Chart 6), we obtain the values for **Zn^{U}Zn^{P}Fb** of $1/L_2 \sim (47/24)(130\ \text{ps}) \sim 250$ ps and for **Zn^{U}Zn^{P}Mg** of $1/L_6 \sim (32/9)(50\ \text{ps}) \sim 180$ ps. We also assume as an initial estimate that L is roughly the same whether the steric hindrance is between zinc porphyrins in **Zn^{D}Zn^{U}Fb** or in the trap subunit in **Zn^{U}Zn^{P}Fb** ($L_2 = L_3$) and, similarly, for **Zn^{D}Zn^{U}Mg** and **Zn^{U}Zn^{P}Mg** ($L_6 = L_7$). We can similarly estimate the effect of steric hindrance on the rate K_{ZnZn} for bidirectional transfer between adjacent zinc porphyrins. In particular, from the dyads (Chart 6), we know that steric hindrance on one aryl ring of the linker slows the unidirectional Zn → Fb transfer by a factor of 2 (**Zn^{P}Fb** versus **Zn^{U}Fb**) and the Zn → Mg transfer by a factor of 3.6 (**Zn^{P}Mg** versus **Zn^{U}Mg**). Thus, an initial estimate is that K_{ZnZn} would be slower by a factor of 1.5−4 when steric hindrance is added between zinc porphyrins.

The above method of estimating nonadjacent energy-transfer rates makes several approximations. (1) The scaling method bases a rate for energy transfer between nonadjacent porphyrins in the triads on the relative transfer rates between adjacent analogous porphyrins in a dyad. The rate in a dyad depends on (the square of) an electronic coupling factor, whereas the rate in a triad will generally depend on two such terms, one for each subunit (Zn−Zn and Zn−trap). Our scaling method for the triads involves a change in only one of the two electronic couplings. (2) The scaling method neglects differences in energy denominators that will come into play in a superexchange description of the nonadjacent transfer process. Despite the limitations of the simple scaling method, the values obtained for the nonadjacent energy transfer were found to be useful for the initial screening of the individual kinetic simulations. Moreover, these values were ultimately found to be consistent with those deduced from the global fits of the energy-transfer dynamics in the arrays.

Appendix 3

Representative Analysis of Individual Arrays. Here, we describe the results of some of the simulations for **Zn^{U}Zn^{U}Mg** and **Zn^{D}Zn^{U}Mg** to convey the logic employed in the analysis. Figure 3 is a contour plot for **Zn^{U}Zn^{U}Mg** ($\tau_R = 20 \pm 5$ ps) and **Zn^{D}Zn^{U}Mg** ($\tau_R = 30 \pm 5$ ps), which uses $1/K_{\text{trap}} = 9$ ps for the Zn → Mg process. For a given pair of values, $1/K_{\text{ZnZn}}$ and $1/L$, the rise time τ_R (the inverse of the smallest nontrivial kinetic eigenvalue) is found on a contour or may be interpolated between contours. One consequence of the nonadjacent energy transfer is that for $1/L < 100$ ps, the observed τ_R is only weakly dependent on $1/K_{\text{ZnZn}}$. This would seem to limit the ability to pinpoint the Zn ↔ Zn energy-transfer rate using this dyad alone. However, closer examination (using the table of calculated results given in the Supporting Information) shows that for the value $1/L_5 \sim 50$ ps estimated above for **Zn^{U}Zn^{U}Mg**, the $\tau_R = 20$ ps target is hit at $1/K_{\text{ZnZn}} \sim 20$ ps with an upper limit at ∼50 ps dictated by the experimental error bar. When $1/L_5$ is doubled to 100 ps, the target is hit at $1/K_{\text{ZnZn}} \sim 10$ ps with an upper limit of ∼20 ps. In the limit that nonadjacent energy transfer does not occur ($L_5 = 0$), the target τ_R is achieved for a very small value of $1/K_{\text{ZnZn}} \sim 4$ ps (as in Figure 1) that is outside the acceptable range when the results for other arrays are taken into account, even including nonadjacent transfer.

The range of acceptable $1/K_{\text{ZnZn}}$ values for **Zn^{U}Zn^{U}Mg** can now be compared with that of **Zn^{D}Zn^{U}Mg**, which differs only in the addition of steric hindrance between the zinc porphyrins. The simple scaling method given above suggests that the $1/K_{\text{ZnZn}}$ should increase by a factor of 1.5−4 and that the nonadjacent transfer should slow to $1/L_7 \sim 180$ ps. The simulations show that the experimental range of $\tau_R = 30 \pm 5$ ps is achieved for a modest span of $1/K_{\text{ZnZn}} = 25-60$ ps for $1/L_7 = 75$ ps, $1/K_{\text{ZnZn}} = 20-35$ ps for $1/L_7 = 170$ ps, and $1/K_{\text{ZnZn}} = 15-30$ ps for $1/L_7 = 340$ ps, with the center target τ_R hit near 40, 30, and 20 ps, respectively, for these three simulation sets. Thus, a modest effect of steric hindrance on the Zn ↔ Zn transfer step is achieved for $1/K_{\text{ZnZn}} = 30-55$ ps for **Zn^{D}Zn^{U}Mg** (with steric hindrance) and $1/K_{\text{ZnZn}} = 10-35$ ps for **Zn^{U}Zn^{U}Mg** (no steric hindrance), and such values occur for values of the nonadjacent transfer (L_7 or L_5) that are reasonable on the basis of the considerations given in Appendix 2.

Supporting Information Available: Complete Experimental Section including procedures for the synthesis of all new compounds, time-resolved absorption data, and kinetic matrices. This material is available free of charge via the Internet at http://pubs.acs.org.

References and Notes

(1) (a) *Anoxygenic Photosynthetic Bacteria*; Blankenship, R. E., Madigan, M. T., Bauer, C. E., Eds.; Kluwer Academic Publishers: Dordrecht, The Netherlands, 1995. (b) Sundström, V.; van Grondelle, R. In *Chlorophylls*; Scheer, H., Ed.; CRC Press: Boca Raton, FL, 1991; pp 1097−1124. (c) Holzwarth, A. R. In *Chlorophylls*; Scheer, H., Ed.; CRC Press: Boca Raton, FL, 1991; pp 1125−1151.

(2) Harvey, P. D. In *The Porphyrin Handbook*; Kadish, K. M., Smith, K. M., Guilard, R., Eds.; Academic Press: San Diego, CA, 2003; Vol. 18, pp 63−250.

(3) Holten, D.; Bocian, D. F.; Lindsey, J. S. *Acc. Chem. Res.* **2002**, *35*, 57−69.

(4) Burrell, A. K.; Officer, D. L.; Plieger, P. G.; Reid, D.-C. W. *Chem. Rev.* **2001**, *101*, 2751−2796.

(5) (a) Kim, D.; Osuka, A. *J. Phys. Chem. A* **2003**, *107*, 8791−8816. (b) Aratani, N.; Osuka, A. *Macromol. Rapid Commun.* **2001**, *22*, 725−740.

(6) (a) Gust, D.; Moore, T. A.; Moore, A. L. *Acc. Chem. Res.* **2001**, *34*, 40−48. (b) Gust, D.; Moore, T. A.; Moore, A. L. *Acc. Chem. Res.* **1993**, *26*, 198−205. (c) Gust, D.; Moore, T. A. *Top. Curr. Chem.* **1991**, *159*, 103−151.

(7) Chambron, J.-C.; Heitz, V.; Sauvage, J.-P. In *The Porphyrin Handbook*; Kadish, K. M., Smith, K. M., Guilard, R., Eds.; Academic Press: San Diego, CA, 2000; Vol. 6, pp 1−42.

(8) Tamiaki, H. *Coord. Chem. Rev.* **1996**, *148*, 183−197.

(9) Gribkova, S. E.; Evstigneeva, R. P.; Luzgina, V. N. *Russ. Chem. Rev.* **1993**, *62*, 963−979.

(10) (a) Wasielewski, M. R. *Chem. Rev.* **1992**, *92*, 435−461. (b) Wasielewski, M. R. In *Chlorophylls*; Scheer, H., Ed.; CRC Press: Boca Raton, FL, 1991; pp 269−286.

(11) Boxer, S. G. *Biochim. Biophys. Acta* **1983**, *726*, 265−292.

(12) Hsiao, J.-S.; Krueger, B. P.; Wagner, R. W.; Johnson, T. E.; Delaney, J. K.; Mauzerall, D. C.; Fleming, G. R.; Lindsey, J. S.; Bocian, D. F.; Donohoe, R. J. *J. Am. Chem. Soc.* **1996**, *118*, 11181−11193.

(13) Wagner, R. W.; Johnson, T. E.; Li, F.; Lindsey, J. S. *J. Org. Chem.* **1995**, *60*, 5266−5273.

(14) Li, F.; Gentemann, S.; Kalsbeck, W. A.; Seth, J.; Lindsey, J. S.; Holten, D.; Bocian, D. F. *J. Mater. Chem.* **1997**, *7*, 1245−1262.

(15) del Rosario Benites, M.; Johnson, T. E.; Weghorn, S.; Yu, L.; Rao, P. D.; Diers, J. R.; Yang, S. I.; Kirmaier, C.; Bocian, D. F.; Holten, D.; Lindsey, J. S. *J. Mater. Chem.* **2002**, *12*, 65−80.

(16) Ambroise, A.; Kirmaier, C.; Wagner, R. W.; Loewe, R. S.; Bocian, D. F.; Holten, D.; Lindsey, J. S. *J. Org. Chem.* **2002**, *67*, 3811−3826.

(17) (a) Lammi, R. K.; Ambroise, A.; Balasubramanian, T.; Wagner, R. W.; Bocian, D. F.; Holten, D.; Lindsey, J. S *J. Am. Chem. Soc.* **2000**, *122*, 7579−7591. (b) Lammi, R. K.; Ambroise, A.; Wagner, R. W.; Diers, J. R.; Bocian, D. F.; Holten, D.; Lindsey, J. S. *Chem. Phys. Lett.* **2001**, *341*, 35−44.

(18) Stryer, L. *Annu. Rev. Biochem.* **1978**, *47*, 819−846.

(19) (a) Rahman, T. S.; Knox, R. S.; Kenkre, V. M. *Chem. Phys.* **1979**, *44*, 197−211. (b) Rahman, T. S.; Knox, R. S.; Kenkre, V. M. *Chem. Phys.* **1979**, *47*, 416. (c) Knox, R. S.; Gülen, D. *Photochem. Photobiol.* **1993**, *57*, 40−43.

(20) Van Patten, P. G.; Shreve, A. P.; Lindsey, J. S.; Donohoe, R. J. *J. Phys. Chem. B* **1998**, *102*, 4209−4216.

(21) Kuciauskas, D.; Liddell, P. A.; Lin, S.; Johnson, T. E.; Weghorn, S. J.; Lindsey, J. S.; Moore, A. L.; Moore, T. A.; Gust, D. *J. Am. Chem. Soc.* **1999**, *121*, 8604−8614.

(22) Yatskou, M. M.; Donker, H.; Novikov, E. G.; Koehorst, R.-B. M.; van Hoek, A.; Apanasovich, V. V.; Schaafsma, T. J. *J. Phys. Chem. A* **2001**, *105*, 9498−9508.

(23) Brodard, P.; Matzinger, S.; Vauthey, E.; Mongin, O.; Papamicaël, C.; Gossauer, A. *J. Phys. Chem. A* **1999**, *103*, 5858−5870.

(24) Hascoat, P.; Yang, S. I.; Lammi, R. K.; Alley, J.; Bocian, D. F.; Lindsey, J. S.; Holten, D. *Inorg. Chem.* **1999**, *38*, 4849−4853.

(25) Wagner, R. W.; Ciringh, Y.; Clausen, C.; Lindsey, J. S. *Chem. Mater.* **1999**, *11*, 2974−2983.

(26) Barshop, B. A.; Wrenn, R. F.; Frieden, C. *Anal. Biochem.* **1983**, *130*, 134−145.

(27) Yang, S. I.; Seth, J.; Strachan, J.-P.; Gentemann, S.; Kim, D.; Holten, D.; Lindsey, J. S.; Bocian, D. F. *J. Porphyrins Phthalocyanines* **1999**, *3*, 117−147.

(28) Gouterman, M. In *The Porphyrins*; Dolphin, D., Ed.; Academic Press: New York, 1978; Vol. 3, pp 1−165.